RSC Advances

PAPER

View Article Online
View Journal | View Issue

Open Access Article. Published on 07 February 2025. Downloaded on 11/7/2025 10:21:52 AM.
This article is licensed under a Creative Commons Attribution-NonCommercial 3.0 Unported Licence.

Check for updates

Cite this: *RSC Adv.*, 2025, **15**, 4163

Performance comparison of nano-Al_2O_3-modified PVDF membranes fabricated *via* two methods for enhanced dye removal†

Runze Liu,[a] Jing Yang,*[a] Ruifeng Zhang,[a] Hongji Li[a] and Ruihua Mu[b]

Received 6th December 2024
Accepted 24th January 2025

DOI: 10.1039/d4ra08615e

rsc.li/rsc-advances

Improving the contamination resistance of polyvinylidene fluoride (PVDF) ultrafiltration (UF) membranes against organic dyes is essential for efficient dye wastewater treatment. In this work, PVDF membranes were prepared using a phase separation method *via* two separate processes (one utilizing Al_2O_3 sol and the other utilizing nano-Al_2O_3 powder-modified PVDF UF membranes), and their anti-pollution ability and enhanced hydrophilicity were evaluated. The effects of the varying content of Al_2O_3 nanoparticles on the microstructure of PVDF membrane were investigated using X-ray diffraction (XRD), scanning electron microscopy (SEM), and Fourier transform infrared spectroscopy (FTIR). Compared to 1.0 wt% Al_2O_3 powder, the modification impact of 20% Al_2O_3 sol on the overall performance of the membrane was superior. It was demonstrated that the pore size and mechanical strength of the modified membranes were notably better than those of the pure PVDF membrane and the water flux also increased from 148.80 L m^{-2} h^{-1} to 217.00 L m^{-2} h^{-1}. An efficient and economical membrane separation method was essential for the treatment of dye wastewater, and the dye filtration experiments revealed that the filtration and antifouling properties of the modified PVDF membranes were significantly improved. The retention rate of Al_2O_3/PVDF-modified membranes for neutral red 5 (NR 5) and dispersed navy blue 79 (DB 79) was more than 96%. After three filtration cycles, the recovery rates of NR 5, DB 79, and bovine serum albumin (BSA) flux were 94.67%, 92.54%, and 95.55%, respectively. These results show that the Al_2O_3/PVDF-modified membranes can cope with more complex wastewater treatment environments.

1. Introduction

Water scarcity and environmental pollution have become global problems. Dye wastewater is one of the most dangerous industrial wastewaters owing to its toxicity and high salinity.[1] In recent years, membrane separation technology has been increasingly concerned with water treatment and wastewater treatment. PVDF is a widely used polymer material.[2] It has excellent mechanical properties, strong permeability as well as decent thermal stability and chemical stability.[3] At the same time, owing to the strong polarity of polyvinylidene fluoride (PVDF), it easily dissolves in some organic solvents. Owing to its easy contamination by impurities, such as proteins, the membrane flux is also low. The research hotspot in recent years has been to modify the ultrafiltration (UF) membrane for retention of the organic matter in dye wastewater to obtain membranes with excellent performance.[4,5]

Currently, the main methods of modifying PVDF UF membranes are blending modification, chemical grafting, and surface modification.[6,7] Blending modification is considered one of the most effective methods for adjusting the pore structure and hydrophilicity of the membrane.[8] Many modifications have been made, including the incorporation of other materials such as nanoparticles (NPs) and hydrophilic polymers, to enhance their hydrophilicity and reduce pollution effects.[9] NPs and metal oxides are usually used as excellent modifiers to improve the properties of organic materials, such as reduced membrane fouling, mechanical strength, hydrophilicity, and optimization of membrane pore structure[10] Currently, particles such as SiO_2, ZrO_2,[11] Al_2O_3,[12,13] Fe_3O_4 (ref. 14) and TiO_2 are blended singly or synergistically with PVDF to improve its hydrophilicity, permeability and stain resistance of substances.

Al_2O_3 nanoparticles have attracted much attention owing to their chemical stability and suitable mechanical strength. Otitoju *et al.*[15] blended Al_2O_3 with polyethersulfone to produce mixed matrix membranes (MMMs), showing better thermal properties and surface roughness owing to their characteristic

[a]School of Urban Planning and Municipal Engineering, Department of Xi'an Polytechnic University, Xi'an Polytechnic University, 58 Shangu Road, Xi'an 710048, China. E-mail: jingy76@163.com

[b]School of Environment & Chemical Engineering, Xi'an Polytechnic University, Xi'an 710048, China

† Electronic supplementary information (ESI) available. See DOI: https://doi.org/10.1039/d4ra08615e

Open Access Article. Published on 07 February 2025. Downloaded on 11/7/2025 10:21:52 AM.
This article is licensed under a Creative Commons Attribution-NonCommercial 3.0 Unported Licence.

ceramic nature. Hydrophilicity of Al_2O_3 provided a new idea for the modification of PVDF membranes. Yan *et al.*[16] prepared Al_2O_3–PVDF composite membranes, which showed significant differences in surface and intrinsic properties compared to the original PVDF membranes. The improved hydrophilicity of the composite membrane also enhanced the anti-fouling performance. Qin H, *et al.*[17] prepared γ-Al_2O_3 UF membranes with a particle size of 30 nm by a reverse micelle (RMs) modified sol–gel process, with excellent rejection for bovine serum albumin (BSA) and methyl blue with the maximum rejection rates of 96.2% and 96.8%, respectively. Isawi *et al.*[18] modified Al_2O_3 nanocomposite PVDF membranes to improve their antifouling properties and membrane performance. The highest permeate flux of 598 L m^{-2} h^{-1} was obtained and used for organic wastewater treatment. The morphology and structure of PVDF membranes are important factors that determine their performance. The properties of the sol–gel process prepared Al_2O_3, such as the grain size, distribution, and morphology also affect the pore size, porosity, and pore volume of the membranes.[19,20] Due to the poor hydrophilicity and low surface-free energy of PVDF membranes,[21] organic matter and printing and dyeing wastewater membrane fouling is a common problem that increases operating and maintenance costs.[22] Fouling-resistant membranes can also suffer from surface fouling during extended operations. Therefore, there is still a great demand for fouling-resistant membranes with good self-cleaning ability and high flux recovery. Studies show that some emerging methods such as tailoring membrane structures and developing flexible membranes for precise separation improve Al_2O_3 membrane performance.[23]

Inspired by the above reports, modifying PVDF membranes by two methods of Al_2O_3 nanoparticles provides a new idea for removing dyes from water. In this research, modifying PVDF membranes were innovatively mixed with different ratios (one utilizing alumina gel and the other from non-gelled inorganic nano-alumina particles modified PVDF membranes) to compare dye removal of the membrane. The surface morphology, hydrophilicity, mechanical strength and permeability of two kinds of membranes were studied in detail. It also elucidates the retention mechanism of the modified membranes when treating different dye solutions. Meanwhile, antifouling properties of the modified membranes in treating organic dye solutions and bovine serum albumin (BSA) were also studied. This study observed high dye rejection performance, indicating that the prepared Al_2O_3/PVDF membranes show great potential for application to promote a sustainable process for dye wastewater treatment.[7,24]

2. Materials and methods

2.1. Preparation of Al_2O_3 sol

To obtain the Al_2O_3 sol, the steps involved in the preparation are outlined below. Sol–gels were prepared using AIP (Chengdu Chron Chemicals Co., Ltd) as the precursor and nitric acid (HNO_3) and water (H_2O) as solvents according to the reactant molar ratio of AIP/HO/HNO_3 = 1/100/0.25. The weighed AIP powder was slowly added to distilled water at 80 °C in a three-necked flask and stirred vigorously for 90 minutes to ensure adequate hydrolysis. Next, using a constant pressure funnel, diluted concentrated 1 mol L^{-1} nitric acid was slowly added drop by drop to the reaction system. The light blue Al_2O_3 sol was prepared that was stable and well distributed after being heated to 85 °C with reflux stirring and maintained under condensation reflux for 8 h.

2.2. Preparation of Al_2O_3 powder

To obtain the Al_2O_3 powder, the gel was dried at 60 °C for 2 h to evaporate water, and the prepared sol was freeze-dried for 24 h and then ground. After that the freeze-dried material was then calcined in a muffle furnace at 1 °C min^{-1} to 500 Celsius for 2 h and then reduced to room temperature to obtain nanoparticles; finally, nano-aluminum trioxide powder was obtained by grinding. In this study, Al_2O_3 powders and sols with different particle size distributions were prepared, as shown in Fig. 1. The average particle sizes were 77.02 nm and 10.69 nm obtained by dispersion in mixed solvents and sonication for 30 min, respectively.

2.3. Preparation of two Al_2O_3/PVDF membranes

For pure PVDF membranes, the casting solution was prepared *via* nonsolvent-induced phase separation (NIPS). The PVDF membrane was cast from a uniform polymer solution containing 14 wt% PVDF powder (FR904, molecular weight (M_w) = 300 000 g mol^{-1}, from Shanghai 3F Co., Ltd) using 85 wt% *N*-methylpyrrolidone (NMP) (Tianjin Fuyu Fine Chemical Co., Ltd) as a solvent to prepare the PVDF membranes with large pore size and high hydrophilicity.[25] The addition of 1 wt% LiCl (Tianjin Kemiou Chemical Reagent Co., Ltd) increases the membrane's mechanical strength and penetration flow.

The preparation process of the two Al_2O_3/PVDF membranes is shown in Fig. 2. In the first step, a certain amount of LiCl was added to the NMP solvent and stirred to obtain a mixed solution. Secondly, a quantity of the prepared Al_2O_3 powder was added to the solvent and stirred for 2 h to disperse. In the third step, the PVDF powder was poured into the above solution in a transparent glass bottle until a complete casting solution was formed, slowly heated at 80 °C for 8 h with constant stirring until a homogeneous solution was obtained. The PVDF powder was vacuum-dried at 80 °C for 24 h before use and then removed for use. During the fourth step, the air bubbles are removed from the casting solution in a vacuum oven for 24 h. The solution was degassed in a vacuum-drying oven at 60 °C for

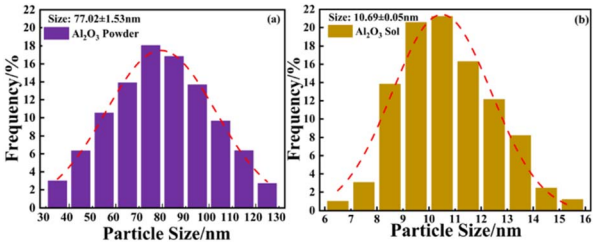

Fig. 1 Particle size distribution of Al_2O_3 powders (a) and sol (b).

 © 2025 The Author(s). Published by the Royal Society of Chemistry

Open Access Article. Published on 07 February 2025. Downloaded on 11/7/2025 10:21:52 AM.
This article is licensed under a Creative Commons Attribution-NonCommercial 3.0 Unported Licence.

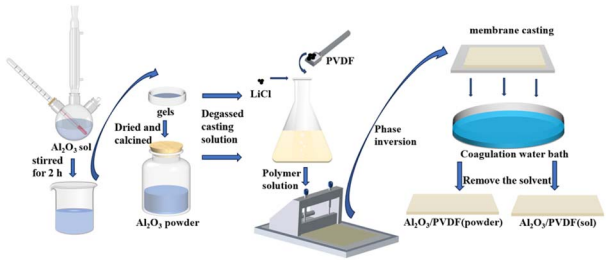

Fig. 2 Schematic of the two Al_2O_3/PVDF membrane preparation processes.

24 h. Then, the degassed casting solution was evenly scraped into a thin membrane with thickness of 100 μm on a glass plate, and after standing in the air for 30 s, it was then transferred to deionized water to remove the solvent. The membrane prepared was dried and named Al_2O_3/PVDF (powder). Membranes doped with Al_2O_3 sol were prepared by the same procedure as a reference and were named Al_2O_3/PVDF (sol) membranes based on the amount of sol added.

To investigate the effect of the inorganic components on the performance of two Al_2O_3/PVDF membranes preparation, 10 ultrafiltration membranes with different contents are prepared as shown in Table 1.

2.4. Characterization

The average particle diameter of the Al_2O_3 powder and sol was measured using a 90Plus Zeta Particle size analyzer (90Plus, America). Scanning electron microscopy (SEM, FEI Quanta-450-FEG, America) was used to characterize the membranes on the surface and cross-section. The membranes were dried and treated at 60 °C for 24 h before the experiment to remove water from the membranes. The chemical structure of the membrane surface was investigated by Fourier transform infrared spectroscopy (FTIR, Nicolet iS50). The measurement range was from 4000 to 400 cm^{-1} with an accuracy of 4 cm^{-1}. X-ray diffraction (XRD, Miniflex600, Japan) was used to adjust the test angle from 5 to 70° (2θ), and the test speed was 5° per min. The chemical structure of the membrane surface was investigated through a water contact angle meter (WCA, JY-82, Chengde Ding sheng Testing Equipment Co. Ltd, China) to measure and record the number of contact angles, and the WCA of each modified membrane was taken five times, and the final results were averaged to indicate the hydrophilicity of the membrane. The mechanical strength of the membranes was tested using a mechanical testing machine (HK-202A, China) with a tensile speed of 25.0 mm min^{-1}; each sample was tested five times, and the average value was calculated.

Table 1 Detailed chemical composition of membranes

Membrane types	Al_2O_3 (powder/wt%)	(Sol/%)
Al_2O_3/PVDF (powder)	0	—
Al_2O_3/PVDF (powder)-0.5	0.5	—
Al_2O_3/PVDF (powder)-1.0	1.0	—
Al_2O_3/PVDF (powder)-1.5	1.5	—
Al_2O_3/PVDF (powder)-2.0	2.0	—
Al_2O_3/PVDF (sol)-10%	—	10
Al_2O_3/PVDF (sol)-20%	—	20
Al_2O_3/PVDF (sol)-30%	—	30
Al_2O_3/PVDF (sol)-40%	—	40
Al_2O_3/PVDF (sol)-50%	—	50

2.5. Measurement of porosity and mean pore size

The wet and dry weight method was used to determine the overall porosity and pore size of the membrane and divided into squares measuring (40 mm), which were then placed in an oven to dry at 60 °C for 24 h to be weighed and recorded (W_d), and then gently cleansed of any remaining water on its surface using a clean cloth before being weighed (W_w), and the porosity of the membrane ε (%) was calculated by using eqn (1).

$$\varepsilon = \frac{(W_w - W_d) \times \rho_p}{W_w \times \rho_p - (\rho_w - \rho_p) \times W_d} \times 100\% \quad (1)$$

where ε is the porosity (%); the weights of the wet membrane and the dry membrane are W_w and W_d (g), respectively; ρ_p is the dry membrane density (1.77 g m^{-3}); ρ_w is the wet membrane density (1.0 g m^{-3}).

Through pure water flux and porosity data, the mean pore size (r_m) of the membrane (nm) was calculated by the Guerout–Elford–Ferry equation eqn (2):

$$r_m = \sqrt{\frac{(2.9 - 1.75 \times \varepsilon) \times 8\mu LJ}{\varepsilon A \Delta P}} \quad (2)$$

where A represents the effective area (cm^2); μ is the viscosity of water (8.9×10^{-4} Pa s, 20 °C); L is the thickness of the membrane (cm); J is the pure water flux (m^3 s^{-1}); ΔP is the change in the transmembrane pressure (0.1 MPa).

2.6. Filtration experiments

Our lab-built staggered flow ultrafiltration equipment was used to conduct testing on the flux and antifouling properties of pure water. The processed membrane sheet was cut into sheets (40 mm × 60 mm), the filtration pressure was adjusted to 0.15 MPa and pre-pressurized for 15 min, waiting for the filtration water pressure to be stabilized and then timed and carried out the flux test experiments, and the pure water flux of the membrane, after the flux was stabilized, the pressure was adjusted to 0.1 MPa and the data was recorded.

In the experiments, BSA solution (0.5 g L^{-1}) was used to characterize the rejection rate of PVDF membranes. A 50 mg L^{-1} solution of neutral red 5 (NR 5, $C_{15}H_{17}ClN_4$) and dispersed navy blue 79 (DB 79, $C_{24}H_{27}BrN_6O_{10}$) solution were prepared. NR 5 and DB 79 were purchased from (Tianjin Kemiou Chemical Reagent Co. Ltd, M_w of 288.7 and 639.5 g mol^{-1}, respectively). The chemical structures of the utilized colors are given in Fig. 3.

Where NR 5 was tested at 553 nm, DB 79 at 535 nm, and BSA at 280 nm. Filtration experiments were carried out using the bovine serum blood protein (BSA) solution at a concentration of 500 mg L^{-1} at 0.1 MPa to study the separation and self-cleaning properties of alumina hybrid membranes. The pure water flux

Open Access Article. Published on 07 February 2025. Downloaded on 11/7/2025 10:21:52 AM.
This article is licensed under a Creative Commons Attribution-NonCommercial 3.0 Unported Licence.

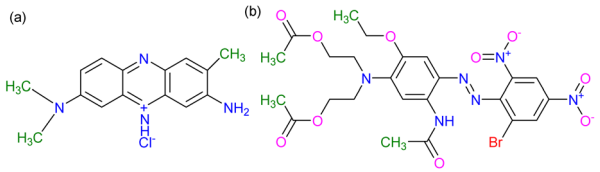

Fig. 3 Chemical structure of neutral red 5 (a) and dispersed navy blue 79 (b).

(J) and rejection rate (R) were calculated as follows using eqn (3) and (4):

$$J = \frac{V}{A \times t} \tag{3}$$

$$R = \left(1 - \frac{C_p}{C_f}\right) \times 100\% \tag{4}$$

where V is the volume of the permeate water (L), A is the effective area of membranes (m^2), t is permeate time (h), C_p and C_f are concentrations of the permeate, and the feed solutions (mg L^{-1}), respectively.

2.7. Antifouling performance evaluation

In the experiments, 50 mg L^{-1} solutions of DB 79 and NR 5 were prepared. The membrane was cut to a size of 4 cm × 4 cm and immersed in 30 mL of dye solution for 24 h at 25 °C. After removing the membrane, a spectrophotometer was used to measure and compute the remaining dye concentration. The adsorption capacity (Q_e, μg cm^{-2}) was calculated using eqn (5).

$$Q_e = \frac{(C_S - C_F) \times V}{A} \tag{5}$$

where Q_e is the adsorption capacity (μg cm^{-2}), C_S is the initial concentration of dyes (mg L^{-1}), C_F is the dye concentration at the end (mg L^{-1}), A is the effective membrane area (cm^2), and V is the volume of the dye solution (L).

After the filtration experiments were completed, the membrane sheet used was washed three times by sufficient shaking for 30 min to remove reversibly adsorbed dye molecules, and pure water flux test experiments were carried out on the membrane sheet again (with a pressure difference of ΔP of 0.1 MPa). The flux recovery rate (FRR) of the membrane was calculated by using eqn (6).

$$\mathrm{FRR} = \frac{J_2}{J_1} \times 100\% \tag{6}$$

where FRR is the flux recovery ratio (%), J_1 and J_2 are the pure water fluxes before filtering and the pure water flux recovery of the membrane (L m^2 h bar), respectively.

3. Results and discussion

3.1. FTIR analysis

To explore the influence of the Al_2O_3 sol and the powder added, FTIR spectroscopy was performed on the functional groups of PVDF membranes and the structures are shown in Fig. 4. The peak at 1404 cm^{-1} for the PVDF membranes corresponds to the stretching vibration absorption of the C–F bond. There is a strong absorption peak at 1176 cm^{-1} in the PVDF membrane, which can be attributed to the deformation stretching vibration of the C–F bond. The pure PVDF membranes are composed of amorphous α-phase and β-phase, where the sharp absorption peaks at 763 cm^{-1} and 603 cm^{-1} are the vibrational absorption peaks of the α-phase, and 1280 cm^{-1} corresponds to the vibrational absorption peak of the β-phase. It can be seen that the spectrum of the PVDF membrane with the added Al_2O_3 nanoparticles changes α-phase and makes the characteristic peaks significantly weaker. In contrast, that of the β crystals increased slightly, which indicated that maintaining the same flow rate and the presence of Al_2O_3 particles changes the stress distribution and crystal structure transformation of PVDF.

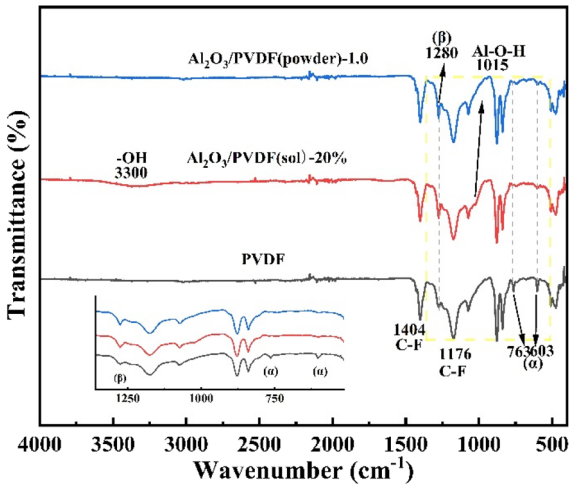

Fig. 4 FT-IR spectra for PVDF pristine membrane and modified membranes by the sol and powder.

Moreover, the band shown at 1015 cm^{-1} is related to the symmetric bending of Al–O–H groups.[26] While the weak bands at 805 cm^{-1} is assigned to the vibration of Al–O in Al_2O_3. Compared with the Al_2O_3 powder, a small amount of water contained in Al_2O_3 20% sol added to the membrane enhances the characteristic absorption peak of –OH at 3300 cm^{-1}. The vibration peak of –OH is not only because the Al_2O_3 surface itself has more carboxyl groups, but also includes the asymmetric stretching vibrations of (Al)O–H and the stretching modes of the adsorbed water. In addition, the presence of these broad bands suggests the characteristics of well-crystallized boehmite structures. Thus, it jointly improves the hydrophilicity of the membrane with oxygen-containing functional groups such as C–O at 1034 cm^{-1}.[27] Comparing the pure PVDF membrane, the prepared Al_2O_3 gel and the nanoparticle-modified PVDF membranes, no new absorption peaks appeared in FTIR, indicating physical mixing without chemical bonding.

3.2. Crystalline structure analysis

To confirm the crystallinity of the modified Al_2O_3 composite, XRD was conducted as shown in Fig. 5. Al_2O_3 has many different crystallographic polymorphs (α, β, γ, δ and ε), and the phase

 © 2025 The Author(s). Published by the Royal Society of Chemistry

Open Access Article. Published on 07 February 2025. Downloaded on 11/7/2025 10:21:52 AM.
This article is licensed under a Creative Commons Attribution-NonCommercial 3.0 Unported Licence.

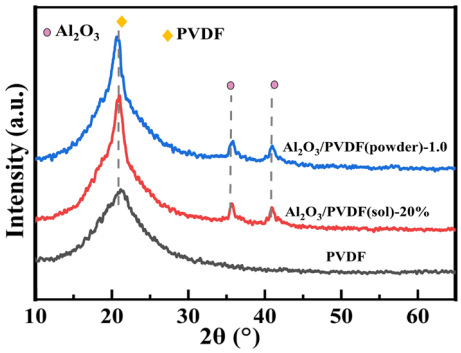

Fig. 5 XRD patterns of PVDF pristine membrane and modified membranes by sol and powder.

transition largely depends on the content and firing temperature of Al_2O_3.[28] It is known that the α-half-crystalline polymer of PVDF membrane is most stable at room temperature. The diffraction peak of the α-crystalline phase appears at $2\theta = 20°$ on the PVDF membrane, which belongs to the refracted reflection surface of (110). It can also be seen that adding different amounts of Al_2O_3 powder and sol that the intensity of the diffraction peak of the α-crystalline phase near $2\theta = 20°$ is not consistent, indicating that the crystallization intensity of the α-crystalline phase at (110) reflection surface inside the membrane is different. In addition, after adding Al_2O_3 nanoparticles, two groups of Al_2O_3/PVDF membranes also showed certain intensity diffraction peaks near $2\theta = 35°$ and 42°, while no diffraction peaks were found in the pure/PVDF membranes at these two positions. This phenomenon indicates that doping Al_2O_3 nanoparticles in the PVDF membrane is beneficial to influencing the generation and change of the crystal phase inside the membrane, which is consistent with the trend of change in the FTIR spectrum. The PVDF membrane added with different amounts of Al_2O_3 powder and sol showed characteristic peaks of Al_2O_3 and PVDF, indicating no significant change in the crystal structure.

3.3. Morphology analysis

SEM images of the surface and cross-section of the pristine PVDF membrane, and modified membranes by the sol and powder are shown in Fig. 6. It can be observed intuitively from a_0 and a_1 that the number of pores on the surface of the unmodified PVDF membrane is small. The cross-sectional image also shows that all three ultrafiltration membranes are typical asymmetric structures with a porous epidermal layer acting as a sieve. The lower layer is a thicker finger-like hollow pore structure, which ensures the permeability of the membrane through small spongy pores in the inner wall.

That is why in the case of Al_2O_3 nanoparticles, the amount of the addition to regulate the size of the pores on the membrane surface can change the pore size and morphology of the PVDF membrane. Fig. 6(b_0 and b_1) shows that Al_2O_3 powder significantly increases the porosity of the membrane surface, and the pore size becomes more uniform. The increase in water flux is mainly due to the rich hydrophilic groups such as hydroxyl groups in Al_2O_3, which causes the H_2O layer to form on the surface of the Al_2O_3/PVDF membrane, reducing the contact angle. This is also conducive to improving the stability of the membrane filtration.

Surface and cross-sectional images of the membrane (doped with 20% Al_2O_3 sol) in Fig. 6(c_0 and c_1) show the increased pore size on the membrane surface compared to that in PVDF membranes. It may be that the addition of Al_2O_3 sol increases the content of the non-solvent in the casting solution system,

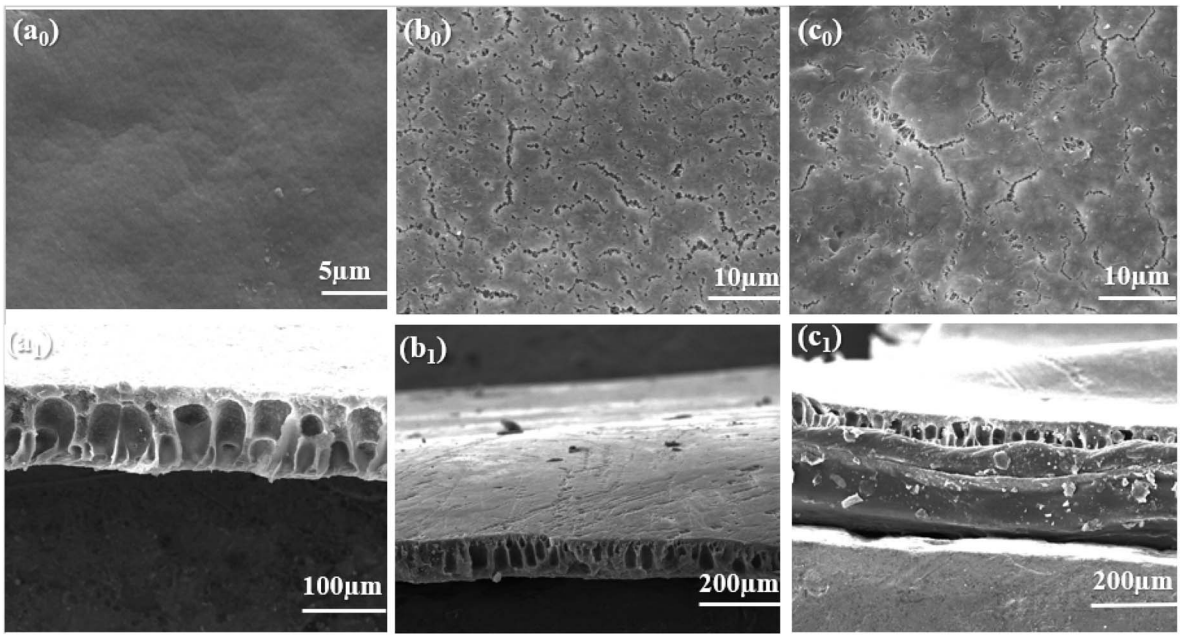

Fig. 6 SEM images of the upper surface and cross-section of membranes: (a_0 and a_1) PVDF membrane; (b_0 and b_1) Al_2O_3/PVDF (powder)-1.0; (c_0 and c_1) Al_2O_3/PVDF (sol)-20%.

Open Access Article. Published on 07 February 2025. Downloaded on 11/7/2025 10:21:52 AM.
This article is licensed under a Creative Commons Attribution-NonCommercial 3.0 Unported Licence.

and PVDF molecules in the system are not easy to aggregate, so the exchange rate between the casting solution system and non-solvent system accelerates, making it easier to form a porous dense and average pore size structure. The Al_2O_3 sol promotes the formation of many finger-like structures inside the membrane. These kinds of finger-like structures are helpful for the rapid penetration of the permeate water in the subsequent filtration tests.

3.4. Mean pore size and porosity analysis

In order to further study the influence of the powder and sol state of the Al_2O_3/PVDF modified membrane on the structure, Fig. 7 shows the porosity and average pore size (r_m) of PVDF membrane. As shown in Fig. 7(a), with the increase of Al_2O_3 powder content, the porosity and average pore size of the modified membrane begin to increase.

When 1% Al_2O_3 powder is added to modify the membrane, the porosity and average pore size of the membrane are 77.30% and 45.02 nm, respectively. This is primarily because the addition of Al_2O_3 powder breaks up the aggregation of PVDF molecules, and there are gaps between the organic phase and inorganic phase during the process of the phase separation, during the membrane formation, which improves the porosity and average pore size of the prepared membrane. The concentration of NPs in Al_2O_3 powders triggers phase coagulation mechanisms, both thermodynamical and rheological, and their presence improves the phase-inversion phenomenon, on the one hand, and induces inhibitory effects, on the other. By going beyond 1% Al_2O_3 powder concentration, for the Al_2O_3/PVDF (powder) membranes, the more the nanoparticles accumulate the less width of the finger pores there would be.

The inclusion of the hydrophilic additives significantly improves the membrane's porosity and average pore size, as seen in Fig. 7(b). Similar results were obtained when Al_2O_3 sol was added using the membrane porosity and average pore size change rule. When adding 40% Al_2O_3 sol to modify the membrane, the porosity and average pore size of the membrane reached a maximum of 81.30% and 49.72 nm, respectively. The shape and particle size distribution of the sol particles are optimized using the sol–gel process, thus optimizing the microstructure of the membrane. When the Al_2O_3 sol is added in excess, the Al_2O_3 sol will also increase the concentration of the polymer in the casting liquid and improve the viscosity of the casting liquid, which will encourage the PVDF molecules to begin to aggregate with each other, affecting the internal structure of the PVDF modified membrane.

3.5. Mechanical strength

The mechanical strength test results of several solvent membranes with varying amounts of Al_2O_3 powder are displayed in Fig. 8(a). The mechanical characteristics of the PVDF hybrid membranes mainly depend on the additives the porosity and pore size distribution of the membrane.[29] Before the modification of the PVDF membrane, the micropores within the LiCl-coated improved the mechanical properties of the membrane. The mechanical characteristics of the membrane with 1.0% doped Al_2O_3 powder were 2.88 MPa; in addition, adding a small amount of Al_2O_3 creates finger-like structures within the membranes that increase tensile strength, however, an excessive addition will weaken the modified membrane's mechanical strength.

Additionally, we can observe from Fig. 8(b) that they attained an optimal value of 3.24 MPa with a 20% addition of the Al_2O_3 sol. The mechanical properties of the polymeric membranes are important parameters for enhanced separation and anti-fouling performance.[30] Additionally, the addition of the correct amount of Al_2O_3 nanoparticles can prevent the production of large holes by the aggregation between the PVDF molecules. The mechanical strength results in an excessive addition that will cause the casting solution to become more viscous, which will result in an uneven distribution of the internal pore sizes. To sum up, the mechanical characteristics of the 20% Al_2O_3 sol-modified membrane are better than those of the Al_2O_3 powder.

3.6. Water contact analysis

Membrane wettability is not only a function of the surface roughness but can also be affected by chemical additions.

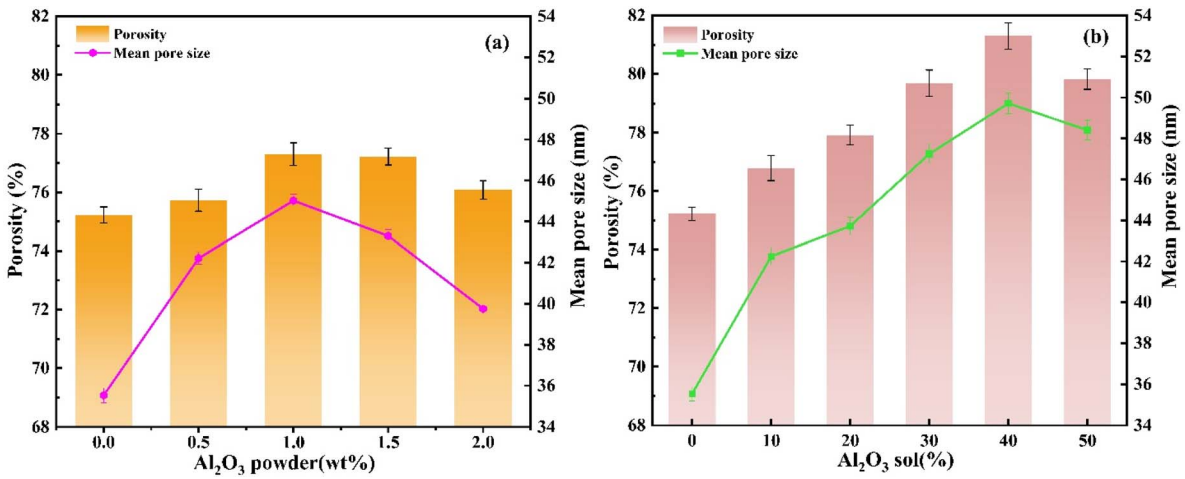

Fig. 7 Effect of the Al_2O_3 content on porosity and average pore size of Al_2O_3/PVDF membranes ((a): Al_2O_3 powder; (b): Al_2O_3 sol).

 © 2025 The Author(s). Published by the Royal Society of Chemistry

Open Access Article. Published on 07 February 2025. Downloaded on 11/7/2025 10:21:52 AM.
This article is licensed under a Creative Commons Attribution-NonCommercial 3.0 Unported Licence.

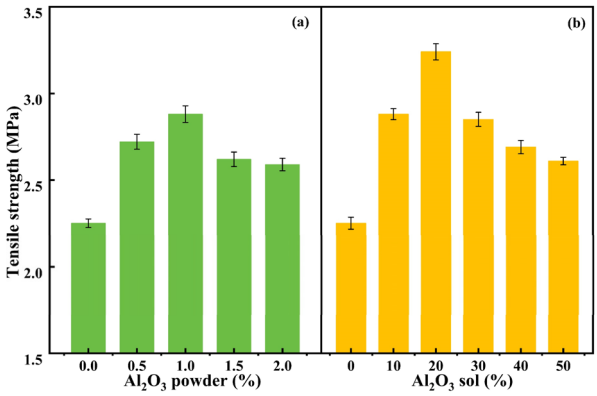

Fig. 8 Effect of Al_2O_3 content on the mechanical strength of Al_2O_3/PVDF membranes ((a): Al_2O_3 powder; (b): Al_2O_3 sol).

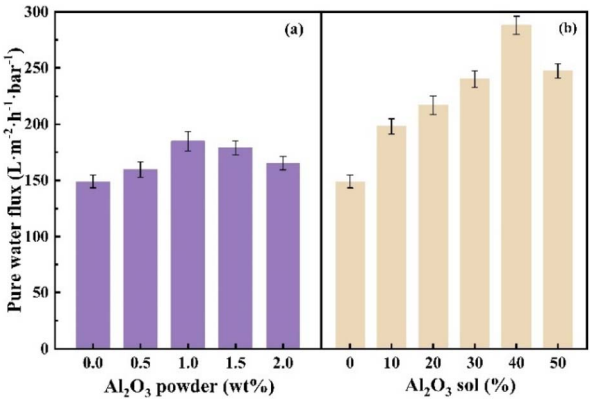

Fig. 10 Effect of content on pure water flux of Al_2O_3/PVDF membranes ((a): Al_2O_3 powder; (b): Al_2O_3 sol).

Through the detection of static water contact angle, the surface hydrophilicity of the PVDF membrane was studied. It can be seen from Fig. 9(a) that the contact angle of the PVDF membrane before adding Al_2O_3 particles was 69°. After adding Al_2O_3 particles, the contact angles of the modified membranes began to decrease, indicating that Al_2O_3 successfully improved the hydrophilicity of the PVDF membrane.[31]

From Fig. 9(b) it can be seen that when using Al_2O_3 sol to modify by adding 40% of it, the pure water contact angle of the membrane is reduced to 62°; the main reason is that Al_2O_3 is rich in hydrophilic groups such as hydroxyl groups. It indicates that the addition of the randomly deposited nanoparticles changes the roughness of the surface hence improving the hydrophobicity of the surface. Generally speaking, increasing the hydrophilicity, porosity, and pore size of the membrane is conducive to increasing the flux.[32] With the increase of the Al_2O_3 content in the membrane, the agglomeration phenomenon begins, which is easy to distribute unevenly and affects the hydrophilic modification effect.

3.7. Membrane filtration performance analysis

As can be seen in Fig. 10, the water flux of the modified membrane with 1.0% of the Al_2O_3 powder was 184.8 L m^{-2} h^{-1}, which was 24.19% higher than that of the PVDF membrane with 148.8 L m^{-2} h^{-1}. The permeability is the ability of the fluid to pass through the porous structure of the membrane. Both water flux and permeability depend on the porosity of the membrane. Obviously, the water flux is higher for a membrane with high porosity.[33] With the increase in the content of the Al_2O_3 powder, the pure water flux showed a tendency to increase and then decrease, which may be due to the fact that the Al_2O_3 powder itself began to aggregate and the hydrophilic effect was weakened. After adding 20% of the Al_2O_3 sol, the water flux was 217.00 L m^{-2} h^{-1}, which may be because PVDF itself behaves as a hydrophobic material, the water flux is low, while Al_2O_3 as a hydrophilic material, itself has hydrophilic groups, which can improve the hydrophilicity of the membrane, so that the water molecules can pass through the PVDF membrane more quickly, thus increasing the water flux. With the increase of the Al_2O_3 sol in the system, the water flux reached a peak value of 288.00 L m^{-2} h^{-1} when the sol content increased to 40%, meaning that Al_2O_3/PVDF coating had a higher contact angle and adhesion property. This is due to the decrease in the viscosity of the membrane, which makes it easy to form a large pore-size structure. The addition of Al_2O_3 effectively improves the pore structure of the membrane, resulting in fewer defects in the pore structure of the membrane and more uniform pore size of the membrane, which leads to improved performance of the membrane.

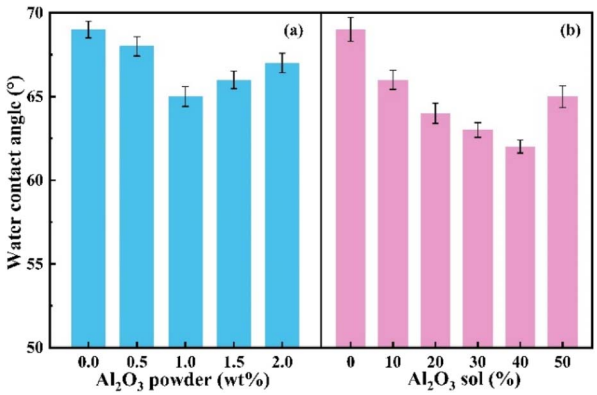

Fig. 9 Effect of Al_2O_3 content on the contact angle of Al_2O_3/PVDF membranes ((a): Al_2O_3 powder; (b): Al_2O_3 sol).

In Fig. 11(a), different PVDF ultrafiltration membranes showed a decreasing trend in the retention of BSA, which is related to the pore size of the ultrafiltration membranes, due to the *in situ* polymerization of the inorganic nanoparticles with PVDF, and the addition of Al_2O_3 made the pore size of the membranes larger. The addition of sols results in a more pronounced reduction in the retention rate. Compared with the membrane before modification, the removal effect of the modified membrane on two dyes removal reached more than 90%. Firstly, the involvement of the OH of the Al_2O_3 sol and the OH aromatic groups of the dye molecules is another reason for improving the dye removal efficiency. The shape and the particle size distribution of the sol particles changed during the sol–gel process, thus optimizing the microstructure of the

Open Access Article. Published on 07 February 2025. Downloaded on 11/7/2025 10:21:52 AM.
This article is licensed under a Creative Commons Attribution-NonCommercial 3.0 Unported Licence.

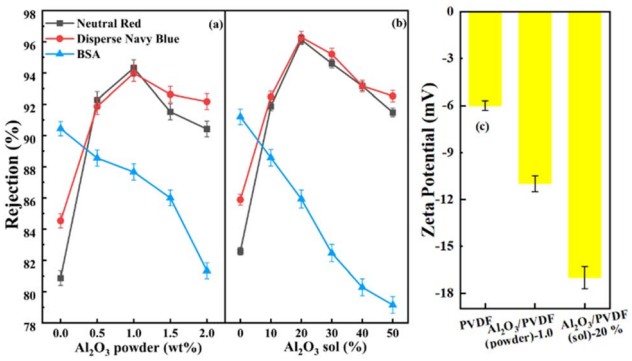

Fig. 11 Effect of the content on filtration performance of Al_2O_3/PVDF membranes ((a): Al_2O_3 powder; (b): Al_2O_3 sol) and zeta potential (c).

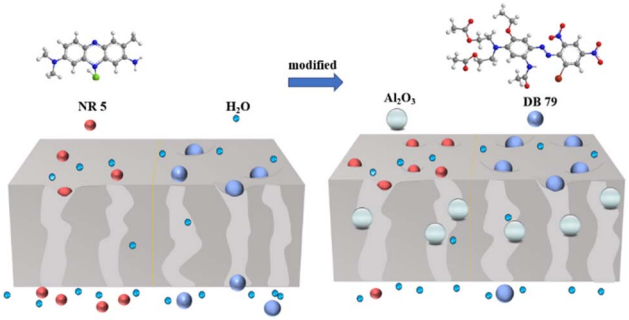

Fig. 12 Schematic of membrane filtration of dyes.

membrane. With the increase in the content, the membrane removal rate of the dye decreased, mainly because the internal structure of the membrane changed, forming a larger pore space in the membrane, the growth in the concentration of nanoparticles not only affects their accumulation but also the membrane morphology. Nanoparticles influence the phase coagulation mechanism both thermodynamically and rheologically and their presence improves the phase-inversion phenomenon, on the one hand, and induces inhibitory effects, on the other. By going beyond this concentration, for the Al_2O_3/PVDF (powder) membranes, the more the nanoparticles accumulate the less width of finger pores would be.[15]

Organic dye removal can be improved by modifying the negative membrane's hydrophilicity and surface charge.[34] The zeta potential change behavior of the three kinds of membranes is shown in Fig. 11(c); the net charge density on PVDF (sol) surface is higher than that of PVDF (powder) because of the introduction of Al_2O_3 sol, which occupied a certain number of positions on the membrane surface that originally belonged to the PVDF resin, which reduced the number of hydrogen bonds between ·F and ·H in organic compounds and improved the negative electric energy on the surface. The effect of Al_2O_3/PVDF (sol)-20% membrane was better, secondly, the retention rate of NR 5 increased from 82.58% to 96.13% and DB 79 increased from 85.88% to 96.29%. Changing the charge of the membrane surface, the dye removal ability of the Al_2O_3/PVDF membrane was enhanced. Moreover, the zeta potential demonstrates that the small charged molecules as dyes do not pass through the membrane, *i.e.* they have higher rejection value when compared to larger uncharged molecules. The rejection of NR 5 (288.7 g mol^{-1}) was high in terms of the M_w of the membrane (300 000 g mol^{-1}). This occurred because these dyes readily formed clusters or aggregates, which enhanced the rejection.

3.8. Antifouling performance analysis

Fig. 12 shows the mechanism of dye retention by the Al_2O_3/PVDF membrane. High PVDF membrane retention rates are associated with molecular sieving action and physical separation.[35] Membrane fouling is one of the most challenging issues for alumina membranes during water purification. During membrane filtration, dyeing wastewater or protein macromolecules in wastewater are deposited on the membrane surface due to complicated physicochemical interactions, resulting in the blockage of the membrane, and consequently causing an irreversible decline in separation performances such as permeability. Mitigating membrane fouling is of great significance for practical applications of alumina membranes.[36] The adsorption capacity of the modified membrane for DB 79 is significantly higher than that for NR 5. On the one hand, DB 79 is a hydrophobic dye molecule that does not contain ionizable water-soluble groups and lower solubility in water and is more readily absorbed into the membrane pores. As DB 79 molecules are difficult to dissolve in water. They are granular in water and will block the tiny pores in the membrane when they enter. On the other hand, NR 5 can be partially ionized under certain conditions to exhibit the nature of a weak cation with a small positive charge, and when in contact with a negatively charged membrane, a strong electrostatic attraction is generated between them. This electrostatic attraction causes the dye molecules to be firmly adsorbed on the surface of the membrane, thus inhibiting the possibility of the dye molecules passing further through the membrane. A dye molecular layer is formed on the membrane surface during the filtration process, and the removal effect is naturally enhanced.

Reversible fouling is usually caused by the deposited solute or colloidal particles on the surface and in the pores. The resulting drop in the flow rate can be easily restored with pure water backwash.[37] Evaluating the anti-fouling and exclusion efficiency of the membrane using the BSA protein solution and the dye solution. It can be seen from Fig. 13 that the addition of Al_2O_3 nanoparticles helps to improve the anti-fouling performance of the membrane. Dye molecules are more easily trapped in small pores inside the membrane. The flux recovery rate of the unmodified membrane after filtering three pollutants is only about 70%. The addition of nanoparticles is best for the flux recovery rate after the modification of the PVDF (sol)-20% membrane. The flux recovery rates after filtering three pollutants are all above 90%, which are NR 5 (94.67%), DB 79 (92.54%), and BSA (95.55%), respectively. The flux recovery effect of other modified membranes is also higher than that before modification, indicating that improving the hydrophilicity of the modified membranes does help to improve their anti-fouling ability, and has no negative effect on the efficiency of the Al_2O_3-doped membranes.

 © 2025 The Author(s). Published by the Royal Society of Chemistry

Open Access Article. Published on 07 February 2025. Downloaded on 11/7/2025 10:21:52 AM.
This article is licensed under a Creative Commons Attribution-NonCommercial 3.0 Unported Licence.

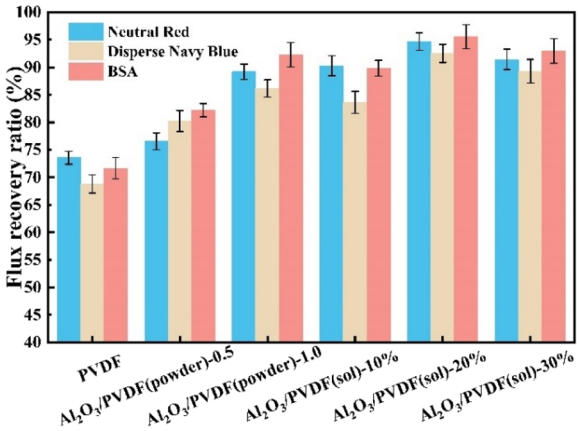

Fig. 13 Effectiveness of different types of Al_2O_3/PVDF membrane flux recovery testing.

Further addition of the Al_2O_3 powder in the membrane will cause agglomeration, destroy the integrity of the membrane pore structure, and result in large pores. When the Al_2O_3 powder content is low (1 wt%), the increase in hydrophilicity and roughness has a synergistic effect on improving the performance of the membrane. In membranes with high concentrations of Al_2O_3 powder, hydrophobic pollutants diffuse longitudinally to the surface of the membrane, causing a decrease in FRR (%). Numerous studies have shown that if the membrane is hydrophilic, its antifouling performance can be more robust.[38] Hydrophilic membrane surfaces are more likely to hydrate by forming hydrogen bonds or electrostatic interactions with water molecules. Further increase in the Al_2O_3 sol content caused by the aggregation tendency of the Al_2O_3 carboxyl groups, making rough-surfaced membranes more susceptible to contamination. Considering the filtration performance of the membrane as a whole, it can be concluded that the 20% PVDF doped sol is the best sol for preparing Al_2O_3/PVDF. In addition, the PVDF-modified membranes are well used at low cost by washing both sides of the membrane surface three times with deionized water when the filtering period is less than 30 min, and the membrane fouling can be almost controlled by choosing an appropriate cleaning method.[39]

4. Conclusions

In this study, nano-Al_2O_3 sol and powder with uniform particle size distribution were prepared. The morphology of the Al_2O_3 particles was controlled during freeze-drying and milling. Two kinds of Al_2O_3/PVDF membranes were synthesized using a phase-inversion process. Prepared membranes were characterized by XRD, FTIR and SEM. The Al_2O_3 sol promoted the formation of many finger-like structures in the membranes, and the subsequent filtration tests proved that such finger-like structures contributed to the rapid passage of permeate water. The modification effect of 20% Al_2O_3 sol was better than that of 1.0% Al_2O_3 powder. The removal rates of the prepared membranes were 96.13% for NR 5 and 96.29% for DB 79. The subsequent filtration experiments proved that the fouling resistance of the two groups of membranes were improved.

Data availability

All relevant data are within the paper. All data supporting the findings of this study are available within the paper and its ESI.†

Author contributions

Runze Liu: conceptualization, methodology, formal, writing. Jing Yang: funding acquisition, review & editing. Hongji Li, Ruifeng Zhang: project administration. Ruihua Mu: methodology.

Conflicts of interest

The authors declare that there are no conflicts of interest.

Acknowledgements

This work was supported by the Key Research and Development Projects of Shaanxi Province, China [2024SF-YBXM-573 and 2023-YBSF-531], the Xi'an Municipal Science and Technology Project, China [23GXFW0023] and the Nature Science Basic Research Plan in Shaanxi Province, China [2024JC-YBQN-0548].

Notes and references

1 W. Ye, J. Lin, R. Borreg, D. Chen, A. Sotto, P. Luis, M. Liu, S. Zhao, C. Y. Tang and B. Van der Bruggen, *Sep. Purif. Technol.*, 2018, **197**, 27–35.
2 H. Mahdavi, N. Zeinalipour, M. A. Kerachian and A. A. Heidari, *J. Water Process. Eng.*, 2022, **46**, 102560.
3 C. Ma, J. Hu, W. Sun, Z. Ma, W. Yang, L. Wang, Z. Ran, B. Zhao, Z. Zhang and H. Zhang, *Chemosphere*, 2020, **253**, 126649.
4 A. Karimi, V. Vatanpour, A. Khataee and M. Safarpour, *J. Ind. Eng. Chem.*, 2019, **73**, 95–105.
5 C. Lavanya, K. Soontarapa, M. S. Jyothi and R. Geetha Balakrishna, *Sep. Purif. Technol.*, 2019, **211**, 348–358.
6 E. J. Sisay, A. F. Fazekas, T. Gyulavari, J. Kopniczky, B. Hopp, G. Vereb and Z. Laszlo, *Membranes*, 2023, **13**, 656.
7 H. Runlin, W. Chaoyue, B. Congcong and W. Hanli, *RSC Adv.*, 2023, **13**, 19002–19010.
8 L. Bai, Y. Liu, A. Ding, N. Ren, G. Li and H. Liang, *Chemosphere*, 2019, **217**, 76–84.
9 R. Gayatri, E. Yuliwati, J. Jaafar, A. N. S. Fizal, M. S. Hossain, M. Zulkifli, A. N. A. Yahaya and W. Taweepreda, *J. Environ. Chem. Eng.*, 2024, **12**, 113276.
10 S. Mohammadpour, P. N. Moghadam and P. Gharbani, *RSC Adv.*, 2024, **14**, 8801–8809.
11 W. Puthai, M. Kanezashi, H. Nagasawa and T. Tsuru, *Sep. Purif. Technol.*, 2024, **333**, 125851.
12 S. Rezaee, K. Ranjbar and A. R. Kiasat, *Ceram. Int.*, 2020, **46**, 893–902.

Open Access Article. Published on 07 February 2025. Downloaded on 11/7/2025 10:21:52 AM.
This article is licensed under a Creative Commons Attribution-NonCommercial 3.0 Unported Licence.

13 H. Xu, R. Luo, Z. Li, Z. Yan, Y. Zhao and H. Su, *Mater. Today Chem.*, 2024, **38**, 102066.
14 Z.-H. Huang, X. Zhang, Y.-X. Wang, J.-Y. Sun, H. Zhang, W.-L. Liu, M.-P. Li, X.-H. Ma and Z.-L. Xu, *Environ. Res.*, 2020, **187**, 109617.
15 T. A. Otitoju, M. Ahmadipour, S. Li, N. F. Shoparwe, L. X. Jie and A. L. Owolabi, *J. Water Process. Eng.*, 2020, **36**, 101356.
16 L. Yan, Y. S. Li, C. B. Xiang and S. Xianda, *J. Membr. Sci.*, 2006, **276**, 162–167.
17 H. Qin, W. Guo and H. Xiao, *Ceram. Int.*, 2019, **45**, 22783–22792.
18 H. Isawi, *J. Water Process. Eng.*, 2019, **31**, 100833.
19 M. A. Tofighy, T. Mohammadi and M. H. Sadeghi, *J. Appl. Polym. Sci.*, 2021, **138**, e49718.
20 Y.-C. Lin, H.-H. Tseng and D. K. Wang, *J. Membr. Sci.*, 2021, **618**, 118729.
21 J. Ren, W. Xia, X. Feng and Y. Zhao, *Mater. Lett.*, 2022, **307**, 130981.
22 Y. Shi, J. Huang, G. Zeng, W. Cheng, J. Hu, L. Shi and K. Yi, *Chemosphere*, 2019, **230**, 40–50.
23 Y. Wang, B. Ma, M. Ulbricht, Y. Dong and X. Zhao, *Water Res.*, 2022, **226**, 119173.
24 N. H. Ismail, W. N. W. Salleh, A. F. Ismail, H. Hasbullah, N. Yusof, F. Aziz and J. Jaafar, *Sep. Purif. Technol.*, 2020, **233**, 116007.
25 F. Russo, C. Ursino, E. Avruscio, G. Desiderio, A. Perrone, S. Santoro, F. Galiano and A. Figoli, *Membranes*, 2020, **10**, 36.
26 S. Anisah, M. Kanezashi, H. Nagasawa and T. Tsuru, *J. Membr. Sci.*, 2020, **611**, 118401.
27 J. Li, S. Guo, Z. Xu, J. Li, Z. Pan, Z. Du and F. Cheng, *J. Membr. Sci.*, 2019, **574**, 349–357.
28 H. Liu, C. Liu, Y. Zhou, Y. Zhang, W. Deng, G. Zou, H. Hou and X. Ji, *Energy Stor. Mater*, 2024, **71**, 103575.
29 A. Mohamed, S. Yousef and M. A. Abdelnaby, *Int. J. Mech. Sci.*, 2021, **204**, 106568.
30 D. Rana, K. Cho, T. Woo, B. H. Lee and S. Choe, *J. Appl. Polym. Sci.*, 1999, **74**, 1169–1177.
31 X. Zhuang, E. Magnone, S. W. Han and J. H. Park, *Ceram. Int.*, 2024, **50**, 24801–24814.
32 M. Khraisheh, F. AlMomani and M. Al-Ghouti, *Int. J. Energy Res.*, 2021, **45**, 8151–8167.
33 M. A. Hussein, H. K. Shahzad, F. Patel, M. A. Atieh, N. Al-Aqeeli, T. N. Baroud and T. Laoui, *Nanomaterials*, 2020, **10**, 845.
34 F. Khoerunnisa, W. Rahmah, B. Seng Ooi, E. Dwihermiati, N. Nashrah, S. Fatimah, Y. G. Ko and E.-P. Ng, *J. Environ. Chem. Eng.*, 2020, **8**, 103686.
35 S. M. Hosseinifard, M. A. Aroon and B. Dahrazma, *Sep. Purif. Technol.*, 2020, **251**, 117294.
36 M. Zhang, H. Ning, J. Shang, F. Liu and S. Peng, *Sep. Purif. Technol.*, 2024, **328**, 124864.
37 L. Yan, S. Hong, M. L. Li and Y. S. Li, *Sep. Purif. Technol.*, 2009, **66**, 347–352.
38 Z. Lv, P. Xue, T. Xie, J. Zhao, S. Tian, H. Liu, Y. Qi, S. Sun and X. Lv, *Sep. Purif. Technol.*, 2023, **305**, 122516.
39 Y. Ninomiya, K. Kimura, T. Sato, T. Kakuda, M. Kaneda, A. Hafuka and T. Tsuchiya, *Water Res.*, 2020, **181**, 115881.

 © 2025 The Author(s). Published by the Royal Society of Chemistry